nature communications

Article

https://doi.org/10.1038/s41467-025-64026-5

Ddx61-enriched condensates refine heart regeneration programs

Received: 7 February 2024

Accepted: 3 September 2025

Published online: 09 October 2025

Check for updates

Mira I. Pronobis[1,2,3], Sophia DeLuca[4], Siyun Lee[1], Lucas Garcia[2,3], Jianhong Ou[1,5], Nenad Bursac[4] & Kenneth D. Poss[1,5,6]

Gene regulatory mechanisms that underlie tissue regeneration have been largely studied at the level of transcription. Here, proximity labeling methods identify increased presence of the RNA helicase and P-body marker Ddx61 in adult zebrafish cardiomyocytes induced to divide by injury or mitogens. Ddx61 molecules form complex condensates in cardiomyocytes during cardiogenic settings in zebrafish, developing mice, and cultured human cells. *ddx61* mutations disrupt cardiomyocyte proliferation and heart regeneration indices in adult zebrafish, and *DDX6* knockdown reduces proliferation of cultured human cardiomyocytes. During heart regeneration, Ddx61 associates with and is required to restrain expression of mRNA encoding Chordin, a secreted BMP inhibitor that impedes regeneration if present at high levels. Our experiments indicate that mRNA sorting by context-dependent condensates can impact tissue regenerative capacity.

Tissue regeneration is a phenomenon of dynamic, regulated gene expression. Adult tissue retained in a principally functional state for months to years is provoked by injury to increase or decrease the expression of thousands of genes. Regeneration programs are customized for each cell type participating in regeneration, and these programs are modified with time to direct formation, growth, and physiological maturation of new tissue primordia. Underlying these programmatic changes are genome-wide modifications in chromatin structure and contextual activation of enhancer regulatory elements that preferentially direct gene expression during regeneration, recently identified in many species and settings of tissue injury[1–6]. Non-transcriptional modes of gene regulation have been implicated in regeneration, but by comparison are underexplored[7–12].

Here we show that the RNA helicase Ddx61 forms condensates in cardiomyocytes undergoing proliferation during heart regeneration in zebrafish, as well as other cardiogenic contexts in zebrafish, mouse, and human cells. Disruption of Ddx61 impairs cardiomyocyte proliferation and heart regeneration, in part through dysregulating expression of the BMP signaling inhibitor chordin. These findings highlight condensate-mediated mRNA control as a layer of gene regulation that shapes tissue regenerative capacity.

Results

Ddx61 condensates form in adult zebrafish cardiomyocytes during cardiogenic stimuli

Certain non-mammalian vertebrates like zebrafish can regenerate heart muscle with minimal scarring, based on the ability of their cardiomyocytes to reduce contractile function and vigorously divide upon injury[13]. A small number of studies have explored proteomic changes that are associated with cardiomyocyte proliferation during heart regeneration[14–17]. Recently, we applied cell-type proximity labeling methods to capture factors enriched in zebrafish cardiomyocytes during heart regeneration, based on myocardial expression of a promiscuous biotin ligase BirA2[17]. To decouple cardiogenic responses from injury- or stress-induced responses, we used this method to capture cardiomyocyte proteomes from animals subjected to experimental augmentation of the mitogenic influences Nrg1 or Vegfaa via induced cardiac overexpression of transgenes, or hyperactivated

[1]Duke Regeneration Center, Department of Cell Biology, Duke University Medical Center, Durham, NC, USA. [2]Department of Biological Sciences, University of Denver, Denver, CO, USA. [3]Knoebel Institute for Healthy Aging, University of Denver, Denver, CO, USA. [4]Department of Biomedical Engineering, Duke University, Durham, NC, USA. [5]Morgridge Institute for Research, Madison, WI, USA. [6]Department of Cell and Regenerative Biology, University of Wisconsin, Madison, WI, USA. e-mail: kposs@morgridge.org

vitamin D receptor signaling by alfacalcidol treatment, compared to control conditions (Fig. 1A, B and Supplementary Data 1–3)[18–20].

Our analysis identified biological processes and signaling components such as Rho GTPase, chemokines, cytokines, Wnt signaling, and EGF receptor signaling pathways as abundant in each adult context of cardiomyocyte proliferation (Figs. 1C and S1A–S1D)[17,18,21–23]. Assessment of abundant cardiomyocyte proteins identified only one factor showing a greater than 1.5-fold enrichment beyond controls in each experimental condition, the DEAD (Asparagine-Glutamine-Alanine-Asparagine) box helicase 61 (Ddx61) (Figs. 1D and S1E) an ortholog of Ddx6 (Rck/P54—*H. sapiens*/*M. musculus*, Dhh1—*S. cerevisiae*, Me31B—*D. melanogaster*, CGH-1—*C. elegans*, Xp54— *X. laevis*). Although we anticipated identifying many other shared proteins, we suspect that other common factors are present in quantities too low to be detected by proximity labeling in adult zebrafish heart tissue. Ddx6 is recognized for a central role in Processing body (P-body) formation[24–26], which are created by liquid–liquid phase separation (LLPS) and can regulate mRNA degradation, storage, and translation during a variety of events, including stem cell maintenance and renewal[24,25,27–30]. Western blot analysis also demonstrated elevated Ddx61 protein levels under each cardiogenic condition versus uninjured or unstimulated controls (Fig. S1F, G). Thus, cardiomyocyte Ddx61 protein levels are elevated during cardiac hyperplasia in adult zebrafish.

To visualize Ddx61, we performed immunofluorescence (IF) staining with an antibody that recognizes both products of gene duplication, Ddx61 and Ddx6 (usually referred to here as Ddx61). In uninjured hearts, visible Ddx61 presence was low, detectable as faint-staining (near background levels), occasional small foci or puncta. However, after a chamber-wide, diffuse cardiomyocyte ablation injury[31], Ddx61 accumulated in more obvious puncta in regenerating compact and trabecular muscle layers (Fig. 1E). These foci were ~10-fold larger and ~5-fold more prevalent during regeneration compared to detectable Ddx61 foci in controls (Figs. 1F, G and S1H). We also injured hearts by partial apical resection (Fig. S2A[13]), finding the highest Ddx61 presence in and around the injury site at early time-points post resection (3, 7, 14 days post amputation (dpa)), resolving to baseline by 30 dpa (Fig. S2A). Visible Ddx61 puncta were also more prevalent after mitogen exposure (Figs. 1H–K and S2B–SF), with an abundance of large foci localized to the compact layer in ventricles of animals overexpressing *nrg1* or *vegfaa*, the muscle type where cardiac hyperplasia occurs in these contexts (Fig. S2B, C[18,19]). EdU labeling revealed that many cycling cardiomyocytes contained abundant Ddx61 foci (Fig. 1L, arrows vs arrowheads, and S2G), indicating a correlation of punctum size and quantity with active proliferation in cardiomyocytes.

To examine whether Ddx61 puncta have properties of P-bodies, we first tested if they are dependent on the process of translation[32–34]. Regeneration-associated Ddx61 puncta were sensitive to treatment with the translation elongation inhibitor cycloheximide, resolving after 9 h of treatment without detectable alterations in Ddx61 protein levels (Fig. S3A–F). Ddx61 condensates were stimulated to form in cardiomyocytes upon treatment of uninjured animals with puromycin, a response that is typical of P-bodies (Fig. S3G–I[33,35,36]). Based on the high conservation of DDX6 proteins (Fig. S3J), these data suggest that Ddx61 foci are not static protein aggregates, but rather dynamic condensates that can resolve after formation, similar to what has been reported for mammalian and yeast Ddx6. P-bodies were initially implicated in RNA decay by their colocalization with Decapping proteins (Dcp) Dcp1 and Dcp2[25], and the presence of translational suppressor proteins 4E-T and LSM14 and others have implicated P-bodies in mRNA storage[37–40]. To test whether P-body markers associate with Ddx61 foci during regeneration, we assessed expression of Dcp2, 4E-T, and LSM14 after cardiac injury. Unexpectedly, high Dcp2 presence and levels were detected in uninjured hearts, with levels decreasing in cardiomyocytes during regeneration (Fig. S4A–E). Some non-myocardial cells displayed high Dcp2 presence (Fig. S4A, II. arrow). In contrast, the translational repressors 4E-T and LSM14 increased in abundance during regeneration, forming foci in cardiomyocytes reminiscent of Ddx61 (Fig. S5A–E). Co-immunoprecipitation (Co-IP) experiments revealed that while some Dcp2-Ddx61 association was detectable in uninjured hearts, none was detected during heart regeneration (Fig. S4F). Consistent with IF data, Co-IP of Ddx61 during regeneration indicated an enhanced association with 4E-T and LSM14 (Fig. S5F). This suggests that, unlike Dcp2, a key component of the mRNA degradation machinery, 4E-T and LSM14 have an increased interaction with Ddx61 during regeneration. To investigate whether this association occurs within Ddx61 condensates, we generated transgenic fish enabling heat shock-inducible expression of a *ddx61-gfp* fusion gene. A heat shock regimen led to conspicuous accumulation of Ddx61-GFP in Ddx61-positive condensates of 7 dpa ventricles (see Fig. S10A), which we used for co-staining of DCP2, 4E-T, and LSM14. Consistent with our hypothesis, we found that 4E-T and LSM14 colocalized well with Ddx61 condensates, whereas DCP2 exhibited weaker colocalization (Fig. S5G). This reduced colocalization of DCP2 is likely due to decreased protein levels during regeneration described above. These findings suggest that Ddx61 condensates might function as storage compartments, rather than sites of mRNA decay, during heart regeneration.

To visualize the subcellular structure of single Ddx61 condensates, we applied STED microscopy. Whereas condensates in uninjured hearts were typically small (80–100 nm in diameter) (Fig. 1M and Movie S1), 14 dpi cardiomyocytes contained large Ddx61 puncta with internal structure that resembled a constellation of single condensates (Movies S2 and S3). These condensate clusters ranged from 300 to 600 nm in size, which is close to the average size of 500 nm reported for Ddx61 condensates in other systems[41]. This was somewhat surprising, as we expected that small Ddx61 condensates would coarsen into larger condensates during regeneration. These measurements are more accurate than those reported here using confocal microscopy, which has poorer resolution and likely groups multiple condensates and condensate clusters (see Fig. 1E–G vs Fig. 1M). When examining Dcp2 puncta, we found that large complexes 200–600 nm in size displayed a smooth surface and did not appear to consist of aggregated small Dcp2 foci (Fig. S4G and Movie S4). Taken together, our data indicate that Ddx61 condensates group into condensate clusters during heart regeneration that are dynamic, transient P-body structures which primary function is in mRNA storage rather degradation.

Ddx61 is required for heart regeneration programs

Zebrafish have two conserved *ddx6*-related genes, *ddx61* and *ddx6*. While the BioID2 assay detected increased levels of Ddx61 protein only, the antibody we used for Western and IF analyses is expected to recognize both proteins based on their high conservation. To test *ddx6* gene functions during zebrafish heart regeneration, we generated *ddx61* and *ddx6* mutants (*ddx61-KO* or *ddx6-KO*) using CRISPR/Cas9 methods (Fig. 2A, C). For each mutant, we deleted the N-terminal-located intrinsic disordered region (IDR), which has been speculated to play a role in LLPS, and the Q-motif that regulates ATP binding and hydrolysis[42–44]. Cardiac Ddx6/61 protein levels were reduced but not depleted in each of the homozygous mutant genotypes (Fig. S6A, B), likely due to cross-recognition by the anti-Ddx6 antibody. Homozygous *ddx61-KO* or *ddx6-KO* animals survived to adulthood, whereas no viable homozygous *ddx6/ddx61* double mutants were present by 1 day post fertilization ($n = 0$ of 380 embryos resulting from four crosses of male *ddx6-KO*; *ddx61-KO* x female *ddx6*-heterozygote; *ddx61*-heterozygote animals). This is consistent with reports that null *DDX6* mutations are lethal in mice, with developmental defects evident as early as E6.5[28,45]. To assess contributions to regeneration-associated condensates, we resected the ventricular apices of adult *ddx6-KO* or

https://doi.org/10.1038/s41467-025-64026-5

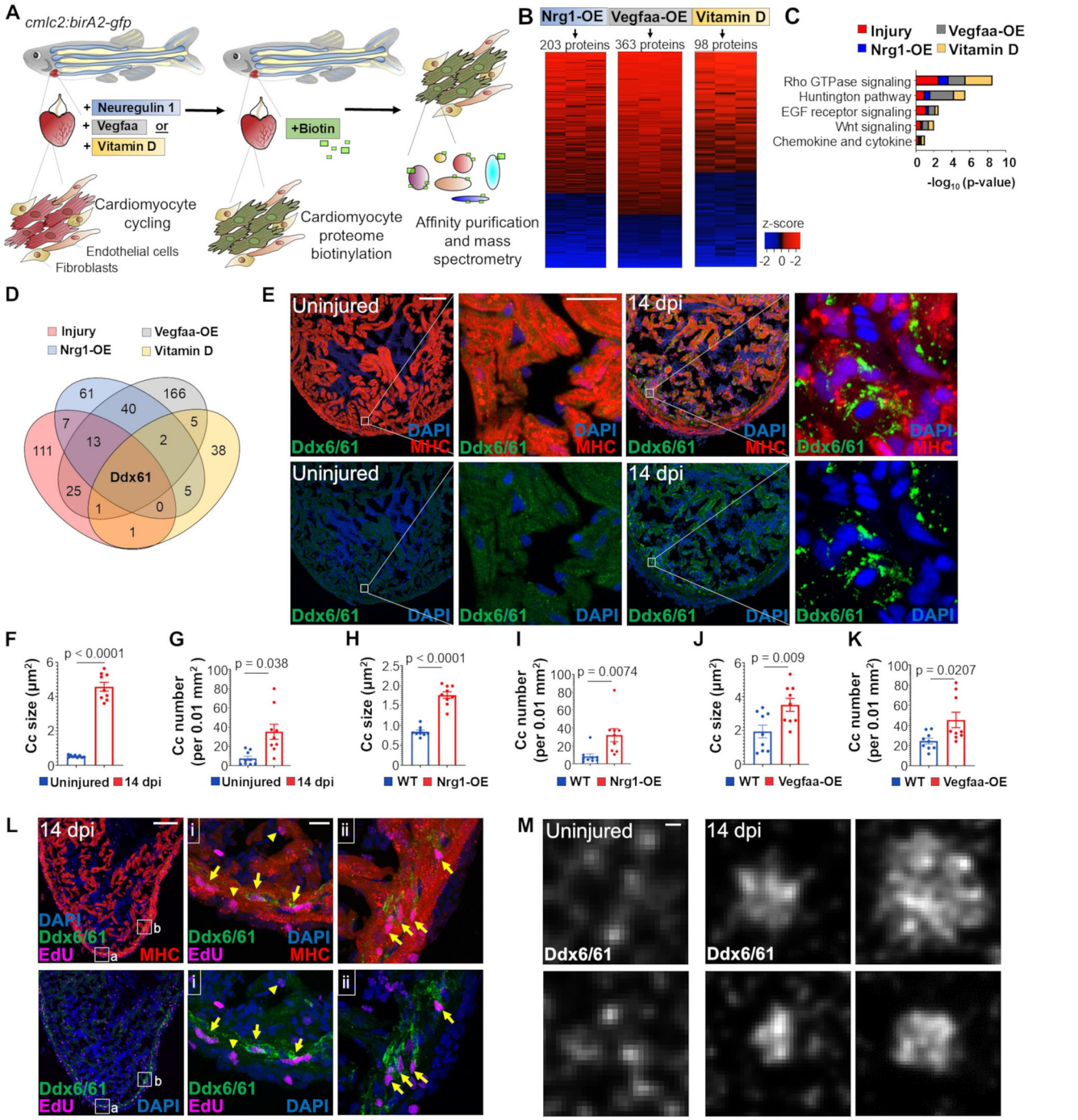

Fig. 1 | Ddx61 condensate responses to cardiogenic stimuli. A Schematic of BioID2 experiment. **B** Heat-map indicating affinity-captured protein level changes in cardiomyocytes after exposure to different cardiac mitogens. **C** Pathway analysis of cardiomyocyte proteins increased 1.5-fold or more during mitogen stimulus or heart regeneration (latter data from ref. 17). **D** Venn diagram of cardiomyocyte proteins increased 1.5-fold or more in each BioID2 context. **E** Immunofluorescence (IF) of sections of uninjured ventricles and those regenerating 14 days after ablation of ~50% of cardiomyocytes (dpi), indicating staining for Ddx61 and myosin heavy chain (MHC). Scale bars, 100 and 10 µm for insets. Quantification of size (**F**) and number (**G**) of Ddx61 puncta (later referred to as condensate cluster (cc)) per 0.01 mm² from sections of uninjured and regenerating hearts. One 100 x 100 µm area was measured per heart (as in Fig. S1H). n = 9 hearts per group. Mean ± S.E.M., two-sided Mann–Whitney U test. Quantification of size (**H**, **J**) and number (**I**, **K**) of Ddx61 puncta (later referred to as condensate cluster (cc)) from sections of Nrg1-overexpressing (**H**, **I**) or Vegfaa-overexpressing (**J**, **K**) hearts or controls. n = 10 hearts per group, three independent experiments. One 100 x 100 µm area was measured per heart. Mean ± S.E.M., two-sided Mann–Whitney U test. **L** IF of sections of 14 dpi ventricles, stained for EdU incorporation to detect cycling cells, as well as Ddx61 and MHC. Arrows, cardiomyocytes with high Ddx61 levels and positive for EdU. Arrowheads, cardiomyocytes labeled with EdU possessing low Ddx61 levels. High magnification views in **i.** and **ii.** Scale bar 100 and 10 µm for insets. **M** STED super resolution images of Ddx61-positive condensates from sections of uninjured or 14 dpi hearts. Image brightness was reduced in 14 dpi images, which conceals single Ddx61 condensates. Scale bar 100 nm. Three independent experiments. Source data are provided as a Source data file.

https://doi.org/10.1038/s41467-025-64026-5

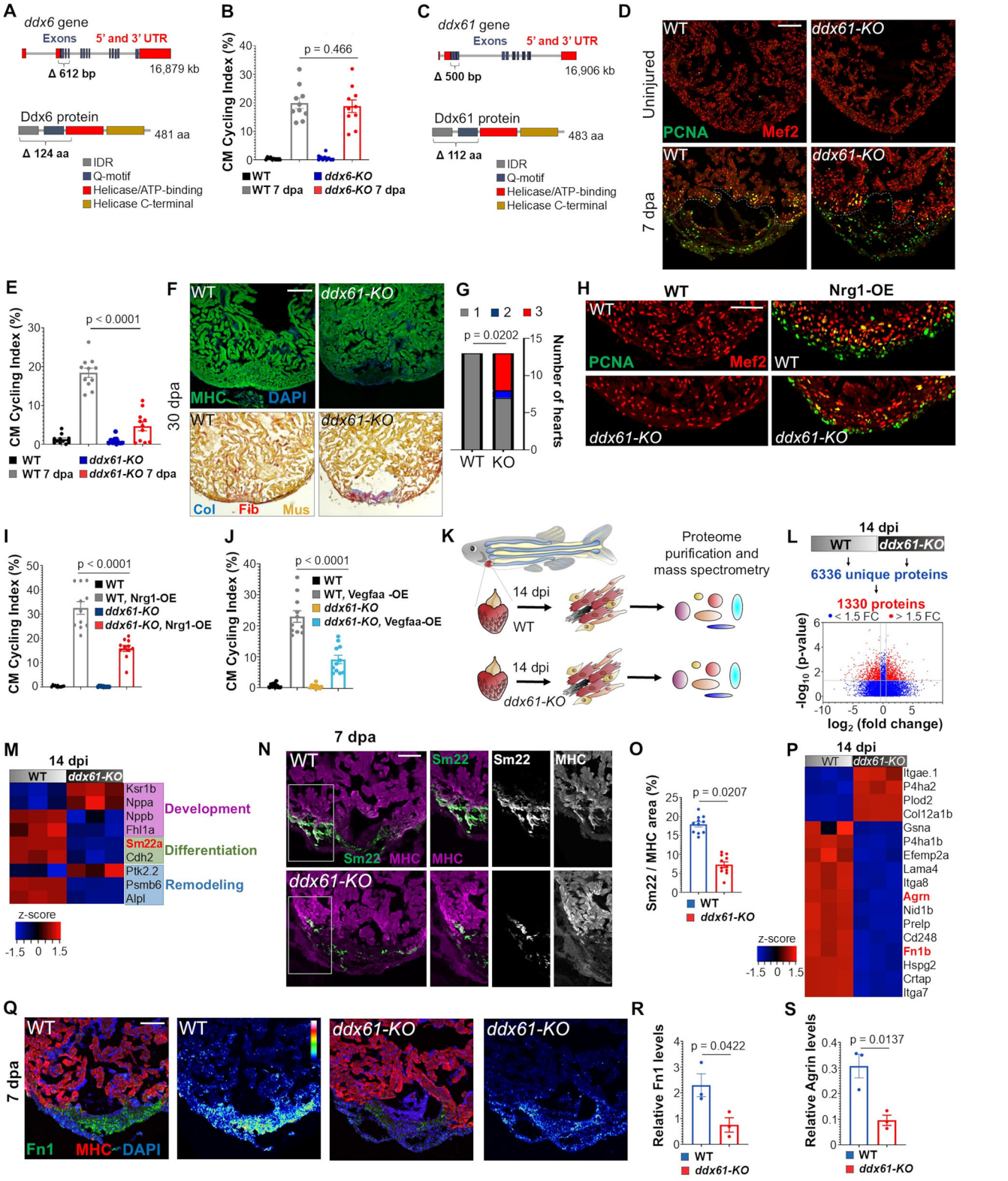

ddx61-KO zebrafish and performed IF staining for Ddx6/61 at 7 dpa. Quantities of Ddx6/61 condensate clusters were sharply reduced in *ddx61-KO* ventricles, and reduced to a much lesser extent in *ddx6-KO* ventricles (Fig. S6D–F). To determine effects of these mutations on heart regeneration, we first assessed mutant animals for proliferative responses of cardiomyocytes to injury. Whereas cycling indices in *ddx6-KO* animals were similar to clutchmate controls (Figs. 2B and S6C), *ddx61* mutations reduced cardiomyocyte cycling to ~1/3rd that of wild-type clutchmates (Fig. 2C–E). We also examined *ddx61-KO* ventricles at 30 dpa for restoration of a contiguous muscle wall, finding that several showed partial or blocked wall regeneration, by comparison with wild-type clutchmates (Figs. 2F, G and S7A, B). *ddx61-KO* animals with only one intact copy of *ddx6* also showed similar or ostensibly more severe defects in regeneration by 30 dpa (Fig. S8A–C).

As Ddx61 condensates also emerge under conditions of enhanced mitogen presence, we also examined effects of *ddx61* mutations on

Fig. 2 | Ddx61 is required for heart regeneration programs. A Schematic of *ddx6* locus. **B** Quantification of PCNA-positive cardiomyocytes in wild-type and *ddx6-KO* ventricles at 7 dpa. n = 10 hearts. Mean ± S.E.M., two-sided Mann–Whitney U test. **C** Schematic of *ddx61* locus. **D** IF images of wild-type or *ddx61-KO* 7 dpa hearts stained for PCNA (green) and Mef2 (red). Scale bar = 100 µm. Three independent experiments. **E** Quantification of PCNA-positive cardiomyocytes (Mef2) in a 100 µm region at the resection site. n = 11 hearts. Mean ± S.E.M., two-sided Mann–Whitney U test. **F** IF (top) and AFOG staining (bottom) of 30 dpa wild-type and *ddx61-KO* ventricles. collagen (Col), fibrin (FN, muscle (Mus). Scale bar = 100 µm. **G** Semi-qualitative scoring of MHC-stained 30 dpa ventricles: complete (1), partial (2), blocked (3) regeneration. n = 13 hearts. Two-sided Fisher's exact test. **H** IF images of wild-type or *ddx61-KO* ventricles with or without *nrg1* overexpression (Nrg1-OE; WT lacks *cmlc2:CreER*, both groups treated with tamoxifen). Scale bar = 100 µm. **I** Quantification from (**H**). n = 11 hearts per group. Mean ± S.E.M., two-sided Mann–Whitney U test. **J** Quantification of cardiomyocyte cycling in wild-type or *ddx61-KO* ventricles with or without *vegfaa* overexpression (Vegfaa-OE). n = 11 hearts. Mean ± S.E.M., two-sided Mann–Whitney U test. **K** Proteome profiling workflow. **L** 1330 proteins were identified with a fold change >1.5. **M** Heatmap shows proteins with fold change >1.5 involved in cardiac development, differentiation, and remodeling. **N** IF of 7 dpa ventricles stained for Sm22 (green) and MHC (magenta). Scale bar = 100 µm. **O** Quantification of Sm22 from (**N**). n = 10 hearts. Mean ± S.E.M., two-sided Mann–Whitney U test. **P** Heatmap of proteins with fold change >1.5 linked to extracellular environment. **Q** IF of 7 dpa ventricles stained for Fn1 (green) and MHC (red). Right: rainbow scale for Fn1. Scale bar = 100 µm. **R**, **S** Quantification of Fn1 and Agrin levels. Western blots in Fig. S9F, H. n = 3 experiments. Mean ± S.E.M., unpaired two-sided *t*-test. Data are provided as Source data.

mitogen-induced cardiomyocyte cycling. We found that induced overexpression of either *nrg1* and *vegfaa* in adult cardiomyocytes had roughly half of their cardiomyogenic effects in the absence of functional *ddx61* (Figs. 2H–J and S9A). In addition to these effects on cardiomyocyte cycling, hyperplastic wall expansion was reduced by 37% and 40% after 14 days of induced overexpression of *nrg1* and *vegfaa*, respectively (Fig. S9B–E). To address whether Ddx61 is sufficient on its own to boost cardiomyocyte cycling, we examined effects of heat shock-induced overexpression of Ddx61 at 7 dpa in transgenic animals. We found no measurable effect of increased Ddx61 presence on cardiomyocyte cycling indices during regeneration (Fig. S10). In cultured pluripotent stem cells, experimental DDX6 increases influenced cell fate decisions[27]. We speculate that the different effects of Ddx61 overexpression are due at least in part to the respective cell differentiation states and tissue environments. Taken together, our data reveal that Ddx61 is required for injury- and mitogen-induced cardiogenesis in adult zebrafish.

To further dissect Ddx61 requirements during heart regeneration, we profiled proteomes of regenerating wild-type and *ddx61-KO* hearts 14 days after partial genetic ablation of myocardium (Figs. 2K, L; S11A and Supplementary Data 4). Gene ontology analysis revealed that proteins associated with mitochondria organization, translational initiation, and glycolysis were dysregulated in *ddx61-KO* ventricles, among other terms (Fig. S11B, C). Datasets gated for cardiac-associated proteins revealed altered levels of factors involved in muscle contraction and cell signaling in *ddx61-KO* hearts (Fig. S11D, E). One of the differential contractile proteins is Smooth muscle protein 22a (Sm22a; also known as Transgelin), a marker of cardiomyocyte dedifferentiation (Fig. 2M[46]). Visualization and quantification indicated a > 50% reduction in *ddx61-KO* cardiac Sm22a levels at 7 dpa compared with wild-types (Figs. 2N, O and S11F, G). Levels of embryonic myosin heavy chain (emMHC) were also reduced by 30% in *ddx61-KO* hearts (Fig. S11I, J). Gating of proteomic data sets for ECM proteins revealed that *ddx61-KO* ventricles have decreased levels of Fibronectin 1b and Agrin -- each of which have been implicated in heart regeneration[15,47], results that were supported by immunodetection (Figs. 2P–S and S11H). Fibronectin is mainly secreted by epicardial cells and their derivatives, and we also observed Ddx61 in epicardial tissue during regeneration (Fig. S11K). Thus, we cannot exclude a model in which Ddx61 regulates ECM proteins in non-myocardial cells, or that ECM dysregulation is secondary to defects in muscle regeneration.

Mammalian DDX6 condensates are associated with less differentiated cardiomyocytes

Cardiomyocytes in humans and mammalian model systems can divide and contribute to hyperplastic cardiac growth at fetal and early postnatal stages. However, in contrast with zebrafish cardiomyocytes, their proliferative capacity tempers as they acquire adult features like increased volume, polyploidy, and a more oxidative metabolic profile[48,49]. To investigate whether DDX6 presence is associated with proliferative capacity in mammalian cardiomyocytes, we first evaluated hearts from different developmental stages in mice, from embryos to adults. We found that prenatal and early postnatal stage ventricles had strong visual presence of DDX6, decreasing when animals reached adulthood (Figs. 3A and S12). Visualization and quantification revealed that condensate cluster number increases from E17.5 to P7, with P7 having the most DDX6 foci (Fig. 3B, C). Cardiomyocyte division is typically minimal after P4, although shifts in gene expression, metabolism, and structural organization continue through P7 as cardiomyocytes mature and increase ploidy[48,50,51]. These events might also involve DDX6 regulation. In P21 and adult hearts, the number of DDX6 clusters decreases considerably (Fig. 3C).

We also examined differentiation of cardiomyocytes in vitro from human induced pluripotent stem cells (iPSCs, Fig. 3D–G). Interestingly, we found that DDX6 condensates were most prominent in mesoderm-like stage D2 cells, and generally present with minor possible fluctuation at other stages (Figs. 3E–G and S13A, B). Super-resolution microscopy revealed that DDX6 condensates also form clusters in hiPSC-derived cardiomyocytes (Fig. S13C. Additionally, FRAP analysis indicated that DDX6 condensates exhibit a dynamic rather than static nature (Fig. S13D, E). IF staining revealed visual colocalization of overexpressed DDX6-RFP with DCP2, LSM14, or 4E-T in D2 and D28 hiPSC cells at moderate incidence (Fig. S14A). To examine functions of human *DDX6* in hiPSC-derived cardiomyocytes, we employed RNAi knockdown in differentiated (D18 and older) cardiomyocytes. Depletion of DDX6 using each of two distinct shRNAs caused a reduction in numbers of condensate clusters and a 40% decrease in cardiomyocyte cycling as measured by flow cytometry (Figs. 3H–N and S14B–E). Interestingly, unlike in zebrafish, overexpression of DDX6 in hiPSC-derived cardiomyocytes resulted in increased cell cycling at D28 (Fig. S14F–I). Taken together, we find that mammalian DDX6 condensates are associated with less differentiated states and earlier stages of cardiomyocyte maturation.

Ddx61 modulates expression of chordin inhibitor during heart regeneration

To attempt to capture mRNAs associated with Ddx61 condensates during zebrafish heart regeneration, we employed eCLIP-seq, a method of antibody pulldown and subsequent cDNA library sequencing (Fig. 4A[52]). A total of 467 genes were represented in profiles of uninjured and regenerating hearts, of which 92 genes fulfilled minimal criteria of at least one read in each of the duplicates and 2 reads per gene (Figs. 4B, S15A and Supplementary Data 5). Our analysis indicated that half of the RNAs we isolated were bound in the CDS regions in uninjured and injured hearts (Fig. 4C). However, while 5′UTR, intron, and 3′UTR regions associated with Ddx61 in samples from uninjured hearts, association with 5′ UTRs was more prominent in regenerating hearts. This might reflect a shift in the mechanism of mRNA recruitment, as both the 5′ and 3′ UTRs play key roles in regulating mRNA recruitment and stability within P-bodies[53,54]. We were unable to identify a common consensus sequence, but when we analyzed these 5′UTRs further, we found that association with 5′UTRs possessing a GC

https://doi.org/10.1038/s41467-025-64026-5

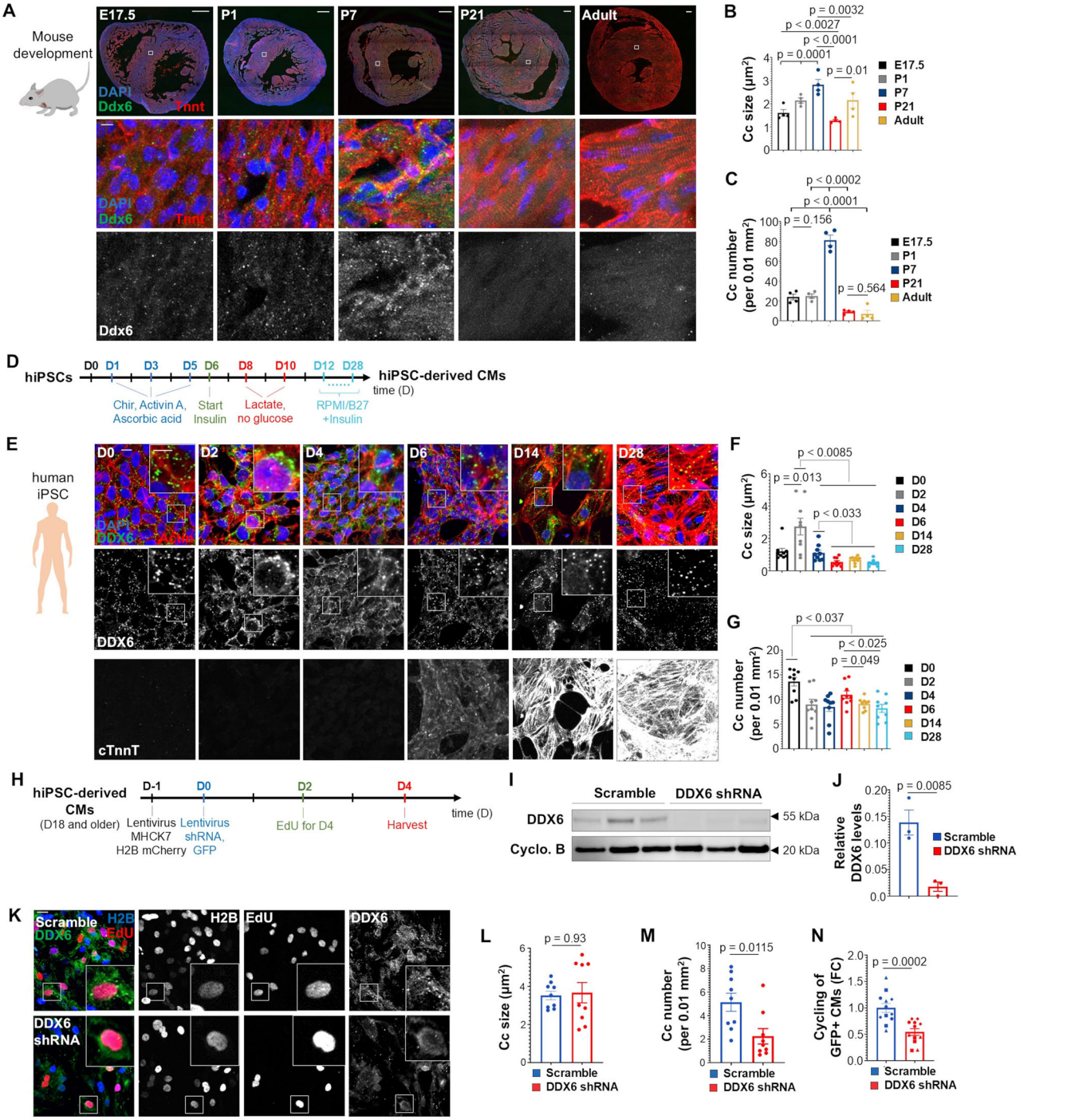

Fig. 3 | DDX6 condensates are associated with less mature cardiomyocytes in mammals. A IF images of transverse sections of developing and adult mouse ventricles stained for DDX6 (green) and Tnnt (red). Scale bar 400 and 5 µm for insets. Quantification of DDX6 condensate cluster (cc) size (**B**) and quantity (**C**) from (**A**). n = 5 animals per group. Mean ± S.E.M., two-sided Mann–Whitney U test. **D** Time course of iPSC culture differentiation. D0, iPSC; D2, mesoderm-like; D4, cardiac "progenitor"; D6, early cardiomyocytes; D14 and D28, iPSC-derived cardiomyocytes (CMs). **E** IF images of human iPSCs undergoing differentiation into CMs. Top: Merge of DDX6 (green), actin (phalloidin, red), and DAPI. Bottom: cardiac troponin t (cTnnT) is shown separately and was not included in merged image. Timepoints are indicated. Scale bar 50 µm. Quantification of DDX6 condensate cluster size by area (µm²) (**F**) and number of DDX6 condensate cluster per 0.01 mm² (**G**). One 0.01 mm² area was imaged and measured per well. n = 9 wells. Mean ± S.E.M., two-sided Mann–Whitney U test. **H** Schematic of *DDX6* knockdown (KD). **I, J** Assessment of *DDX6* knockdown by Western blot analysis and quantification, n = 3 experiments. Mean ± S.E.M., unpaired two-sided *t*-test. **K** IF images of hiPSC-derived CMs treated with scramble or *DDX6* shRNAs stained for DDX6 (green), EdU (red), and H2B (blue, labeling CMs). Scale bar 20 µm. Quantification of size by area (µm²) (**L**) and number (**M**) of DDX61 condensate cluster per 0.01 mm² from images of CMs treated with scramble or *DDX6* shRNA. One 100 x 100 µm region was imaged and measured per well. n = 9 wells. Mean ± S.E.M., two-sided Mann–Whitney U test. **N** Quantification of EdU incorporation in GFP⁺ CMs from Fig. S14D. Knockdown of *DDX6* reduced CM cycling as measured by flow cytometry. Mean ± S.E.M., two-sided Mann–Whitney U test. Source data are provided as a Source data file.

https://doi.org/10.1038/s41467-025-64026-5

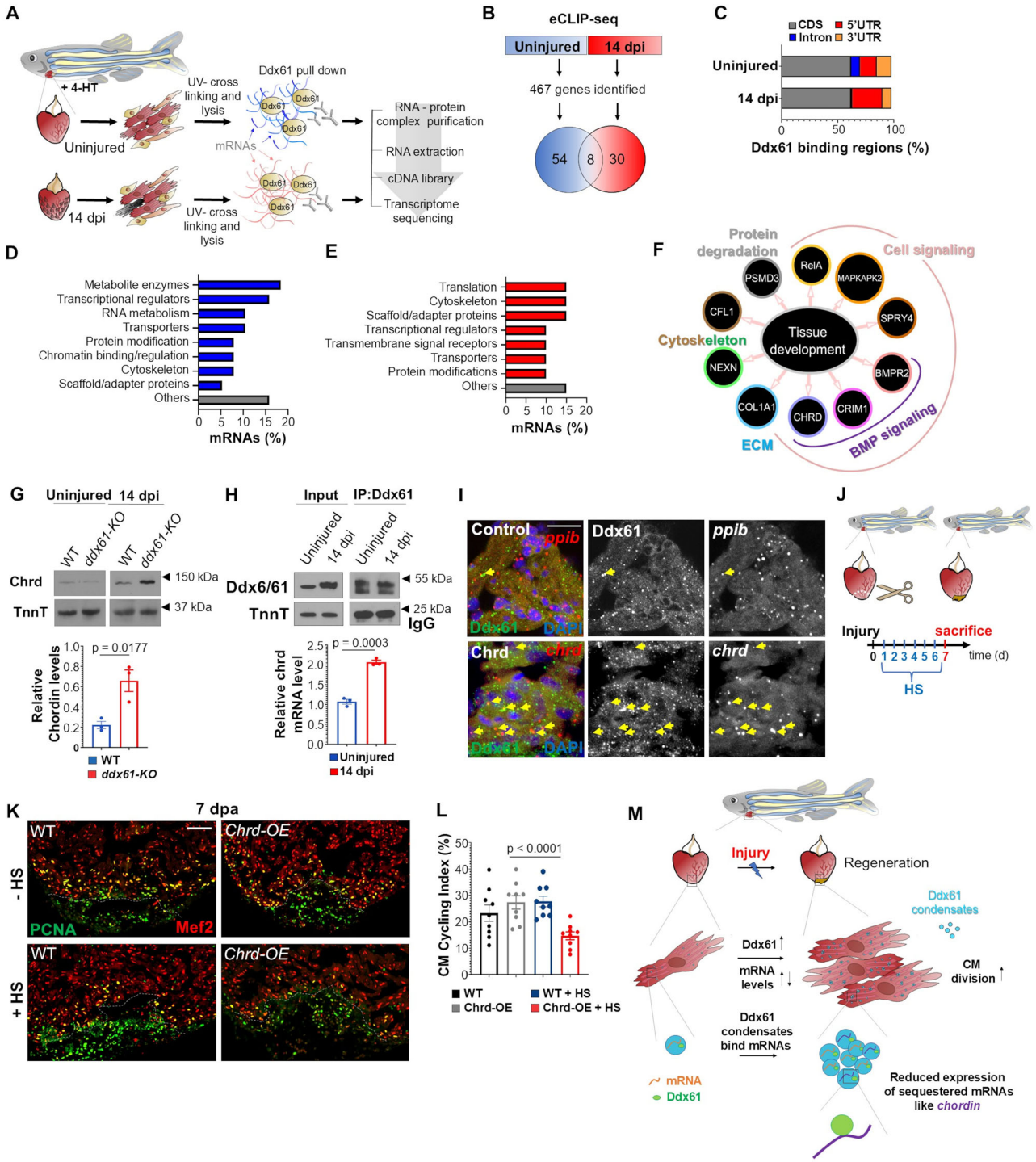

Fig. 4 | Ddx61 modulates signaling events during heart regeneration. **A** Schematic of eCLIP-seq workflow used to identify Ddx61-bound mRNAs. **B** Summary of mRNAs associated with Ddx61 complexes in uninjured and 14 dpi regenerating hearts. **C** Mapping of Ddx61-binding sites across coding sequences (CDS) and untranslated regions (UTRs), showing broad distribution of associations. All transcripts, $p < 0.05$, two-sided Student's t test; FDR < 0.001. Functional classification of Ddx61-associated transcripts in uninjured (**D**) and 14 dpi (**E**) hearts, indicating enrichment of specific cellular processes. $p < 0.001$, two-sided Student's t test; FDR < 0.002. **F** Ten genes were identified in the GO category "tissue development," including *chrd*, *crim1*, and *bmpr2*, which regulate BMP signaling, and *col1a1*, *nexn*, *cfl1*, *psmd3*, *relA*, *mapkapk2*, and *spry4*. $p = 0.05$, FDR < 0.02. **G** Western blot analysis showing increased Chrd protein levels in *ddx61*-KO ventricles after injury (top), with quantification of three independent experiments (bottom). Mean ± S.E.M., unpaired two-tailed t test. **H** RIP assay demonstrating association of Ddx61 with *chrd* mRNA in uninjured and 14 dpi hearts. Western blot of pulldown (top) and RT-qPCR quantification of *chrd* mRNA (bottom). $n = 3$ biological samples, unpaired two-tailed t test; mean ± S.E.M. **I** RNAScope analysis of *chrd* mRNA in ventricular tissue, showing colocalization with Ddx61 protein by antibody staining. A *ppib* probe served as positive control. Arrows indicate regions of colocalization. $n = 9$. **J** Workflow of *chrd* overexpression experiments. Wild-type and *hsp70:chrd* animals underwent partial ventricular resection followed by daily heat-shocks. Hearts were collected at 7 dpa. **K** Immunofluorescence images of *hsp70:chrd* ventricles stained for PCNA (green) and Mef2 (red). Scale bar = 100 µm. **L** Quantification of PCNA-positive cardiomyocytes in a defined region of the resection site from (**J**). $n = 9$ hearts; mean ± S.E.M., unpaired two-tailed t test. **M** Model summarizing Ddx61 function. Following injury, Ddx61 levels increase, accumulate in condensates, and associate with mRNAs to regulate expression, as identified for *chordin*. Source data are provided as a Source data file.

content above 60% was more common in regenerating hearts (Fig. S15B). Interestingly, when we expanded our GC content analysis to all mRNAs, we found more GC-rich messages associated with Ddx61 complexes during regeneration than in the absence of injury (Fig. S15C). In human tissue culture cells (epithelial HEK293T and erythroid K562 cells), P-bodies have been shown to preferentially harbor AU-rich mRNAs that are translational repressed, and selection and repression are dependent on DDX6[55]. Although eCLIP-seq captured only a small subset of mRNAs, we hypothesize that the observed shift of Ddx61-associated transcripts toward GC-rich sequences during regeneration could represent a change in mRNA selection. This shift may also reflect that Ddx61 targets different mRNAs during regeneration, potentially influencing gene expression by favoring GC-rich messages for repression or translation control.

Gene ontology (GO) analysis of the eCLIP-seq dataset revealed enrichments in mRNAs involved in translation, scaffolding/adapter proteins, and cytoskeleton during regeneration, whereas metabolite conversion, transcription, and RNA metabolism were represented in uninjured hearts (Fig. 4D, E). Analysis for biological processes enriched during regeneration from our sampling screen identified 10 Ddx61-associated mRNAs within the GO category tissue development (Fig. 4F). Many proteins that are dysregulated in *ddx61-KO* (described earlier) have reported pathway interactions with products of these mRNAs, including Sm22a (Fig. S16). Two genes encoding mRNAs associated with Ddx61 in the eClip-seq data set exhibited increased protein levels in *ddx61*-KO hearts compared to wild-type hearts during regeneration. Additionally, several genes encoding mRNAs with greater association to Ddx61 in uninjured hearts versus regeneration also expressed higher protein levels in *ddx61-KO* samples compared with wild-types (Supplementary Data 6). Interestingly, three genes, *chordin (chrd)*, *crim* and *bmpr2a* are components of BMP signaling, a pathway that has been reported to be regulated by DDX6 in mammals and also to promote zebrafish heart regeneration[45,56]. Protein levels of chordin and Bmpr2a were elevated in *ddx61-KO* hearts during regeneration compared to wild-type hearts (Figs. 4G and S17A, B). These increases in protein levels were evident even though mRNA levels for these genes were comparable in *ddx61-KO* and wild-type hearts (Fig. S17C, D), consistent with regulation of mRNA translation.

Phospho-SMAD1 levels in *ddx61-KO* regenerating hearts were reduced compared to wild-types, indicating that loss of Ddx61 decreased cardiac BMP activity (Fig. S17E, F), potentially due to increased levels of Chrd. RNA immunoprecipitation (RIP) analysis followed by RT-qPCR further indicating an increased association of *chrd* mRNA with Ddx61 in 14 dpi hearts versus uninjured hearts (Fig. 4H, top and bottom). Moreover, RNAscope analysis indicated frequent colocalization of *chrd* mRNA with Ddx61 clusters, suggesting recruitment of *chrd* mRNA to Ddx61 foci (Figs. 4I and S18A–C). To investigate if other P-body proteins colocalize with Ddx61 clusters and *chrd* mRNA, we used our heat shock-inducible Ddx61 overexpression line, finding that LSM14 colocalized with foci containing both components (Fig. S18D, E). To test whether Ddx61 effects on Chrd protein can impact heart regeneration, we employed a published *hsp70:chrd* transgenic line enabling heat-inducible augmentation of Chrd[57]. We found that daily heat-induced Chrd increases could reduce cardiomyocyte cycling by ~40% at 7 dpa, as well as the incidence of complete myocardial regeneration at 30 days post resection (Figs. 4J–L, S15D–G and S19A–D). Thus, the emergence of Ddx61 condensates during regeneration is accompanied by new mRNA interactions, including that with an inhibitor of BMP signaling that can disrupt regeneration at high levels.

Discussion

Our study reveals a role for Ddx61 biomolecular condensates during cardiac regeneration and expands the regulatory interplay of tissue regeneration to include posttranscriptional mechanisms by ribonucleoprotein granules. DDX6 was reported to regulate stem cell maintenance and fate decisions by association with mRNAs encoding key regulators in human, murine embryonic stem cells, and lineage-specific progenitors[27]. Our study indicates that Ddx61-containing condensates regulate messages during regeneration of a complex organ like the heart, perhaps providing a level of intricacy beyond initial transcriptional control in tissues experiencing profound molecular changes associated with regeneration or rapid tissue growth (Fig. 4M). For instance, Ddx61 condensates might serve as hubs for measured expression of powerful developmental signals, like growth factors, transcription factors, or chromatin regulators. RNA-binding proteins, proteins of the translational machinery, and mRNA degradation machinery could codetermine the fate of key messages as has been reported to occur during early development[58–62]. Deciphering and commandeering the Ddx61 regulatome may provide insights for enhancing human regenerative biology.

Methods

Zebrafish

Zebrafish stains of the Ekkwill (EK) background at the age of 4–12 months were used in this study with a dark/light cycle of 12 h and water temperature of 26 °C. The following published transgenic lines were used in this study: *Tg(cmlc2:CreER)*[31], *Tg(bactin2:loxP-mCherry-STOP-loxP-DTA176)*[31], *Tg(bactin2:loxP-bfp-STOP-loxP-nrg1)*[18], *Tg(bactin2:loxP-bfp-STOP-loxP-vegfaa)*[19], *Tg(cmlc2:bira2-gfp)*[17]. Partial resection of the cardiac ventricle to remove ~20% of the apex was performed as previously described[13].

Biotin injections were performed as previously described[17]. Briefly, 5 µM Biotin solution was injected intraperitoneally (IP) into adult fish on three consecutive days. Alfacalcidol was injected IP 3 days prior to harvest of fish hearts as previously described[20]. Tamoxifen treatment to ablate cardiomyocytes was performed as described previously, by incubating *cmlc2:CreER; βactin2:loxp-mCherry-STOP-loxp-DTA* animals or *cmlc2:CreER*-negative clutchmates in 1–5 µM Tamoxifen (Sigma–Aldrich, St. Louis, MO) for 16 h[31]. Nrg1 and Vegfaa expression were each induced as described by incubating adult *cmlc2:CreER; β-act2:BSnrg1* or *cmlc2:CreER; β-act2:BSvegfaa* animals (*cmlc2:CreER*-negative clutchmates), respectively, in 5 µM Tamoxifen for 24 h[18,19]. Hearts were harvested 14 days after treatment. For Cycloheximide treatment, fish were bathed in 200 µM cycloheximide for 9 h. Puromycin was IP injected and hearts were collected 6 h later. Procedures involving zebrafish were approved by the Institutional Animal Care and Use Committee at Duke University.

Generation of *ddx6-KO* mutants

For *ddx6* mutations, the following two gRNAs were designed to delete 600 bp of the N-terminus: 5′ - CCTGGCCCCTTGTCTGTGAAACT – 3′ and 5′ – CCTTCCCATGTATCAGGCCTGGA – 3′. gRNAs were co-injected with 2 µl Cas9 protein (PNA-Bio) into one-cell stage zebrafish embryos. Fish were screened using forward primer 5′- CTCTAGCACAGTCAACAATGGC –3′ and reverse primer 5′- TGATGTTTTCATTCGCAAATCT –3′. The allele designation for this *ddx6* deletion is *pd396*.

Generation of *ddx61-KO* mutants

To generate *ddx61* mutations, two gRNAs, 5′- CAAGCCCATGAGCCTTCAGACGG – 3′ and 5′ - TAGATTACCTGTATAGGGGAAGG – 3′, were designed to delete 500 bp of the N-terminus of the *ddx61* gene locus. gRNAs were co-injected with Cas9 protein into one-cell stage zebrafish embryos. Fish were screened using forward primer 5′- AGAACTGAGATCCCTGCTTCAG –3′ and reverse primer 5′- TCCATCAATGTCATGAGCAAAT-3′. The allele designation for this *ddx61* deletion is *pd397*.

Generation of *hsp70:ddx61-gfp* animals

For overexpression of *ddx61*, VectorBuilder was used to generate the plasmid I-SceI-*hsp70:ddx61-gfp*. This construct was co-injected with I-Sce-I enzyme mix (1 µl of I-Sce-I, 1.5 µl of buffer in 30 µl of ddH2O) into

one-cell stage embryos. One founder was isolated. The full name of the transgene is *Tg(hsp70:ddx61-gfp)*^{pd398}.

BioID2-based proximity labeling and analysis

Transgenic zebrafish expressing *cmlc2:birA2-gfp* and overexpressing either *nrg1* or *vegfaa*, or treated with vitamin D analog alfacalcidol, were interperitoneally (IP) injected with 10 µl of a 5 µM biotin/PBS solution on three consecutive days before hearts were isolated (15 hearts per sample). Once hearts were extracted, biotinylated proteomes were purified as described previously[17]. Mass spectrometry was performed by Duke Proteomics and Metabolomics core as previously described[17].

The overall the dataset contained 326,390 peptide spectral matches. Additionally, 1,848,788 MS/MS spectra were acquired for peptide sequencing by database searching. Following database searching and peptide scoring using Proteome Discoverer validation, the data were filtered for only *Danio rerio* proteins, casein, and ADH and annotated at a 1% protein false discovery rate, resulting in identification of 1206 proteins. Proteins with $p > 0.05$ and a change ≥1.5 fold were chosen for further analysis. GO analyses were preformed using DAVID Functional Annotation Bioinformatics Microarray Analysis and PANTHER knowledgebase.

Proteomic profiling of *ddx61-KO* ventricles

To injure hearts, *ddx61-KO* were crossed to the Z-CAT ablation model system in which the DTA toxin is inducibly expressed in a portion of cardiomyocytes, as previously described[31]. Protein purifications were performed on uninjured and 14 dpi hearts from wild-type or *ddx61-KO*. Per sample, 25 hearts of 3–8 month old fish were collected in RIPA lysis buffer (10 mM Tris-HCL, 1 mM EDTA pH 8.0, 1% Triton-X-100, 0.1% SDS, 0.1% Sodium deoxycholate, 140 mM NaCl, 100x Proteinase and Phosphatase inhibitor, and protease inhibitor PSMF). Next, hearts were homogenized using an Eppendorf tube pestle and flash frozen. Samples were incubated on ice for 15 min and again homogenized by a tube pestle. Samples were centrifuged at 20,000 x *g* for 25 min at 4 °C, and supernatants were moved into fresh tubes and sent to the Duke Proteomics and Metabolomics core for mass spectrometry analysis.

Protein concentrations were determined via BCA and ranged from 2.745 to 3.777 µg/µL. Samples were normalized to 30 µg and spiked with undigested bovine casein at a total of either 2 or 4 pmol as an internal quality control standard. Next, samples were supplemented with 7 µL of 20% SDS, reduced with 10 mM dithiolthreitol for 15 min at 80 °C, alkylated with 20 mM iodoacetamide for 30 min at RT, then supplemented with a final concentration of 1.2% phosphoric acid and 418 µL of S-Trap (Protifi) binding buffer (90% MeOH/100 mM TEAB). Proteins were trapped on the S-Trap micro cartridge, digested using 60 ng/µL sequencing grade trypsin (Promega) for 1 h at 47 °C, and eluted using 50 mM TEAB, followed by 0.2% FA, and lastly by 50% ACN/0.2% FA. All samples were frozen and lyophilized to dryness. Samples were resuspended in 60 µL of 1% TFA/2% acetonitrile with 12.5 fmol/µL of yeast alcohol dehydrogenase (ADH).

Quantitative LC/MS/MS was performed with 2 µL of each sample, using an MClass UPLC system (Waters Corp) coupled to a Thermo Orbitrap Fusion Lumos high resolution accurate mass tandem mass spectrometer equipped with a FAIMSPro device via a nanoelectrospray ionization source. Briefly, the sample was first trapped on a Symmetry C18 20 mm × 180 µm column (5 µl/min at 99.9/0.1 v/v water/acetonitrile), after which the analytical separation was performed using a 1.8 µm Acquity HSS T3 C18 75 µm × 250 mm column (Waters Corp.) with a 90-min linear gradient of 5–30% acetonitrile with 0.1% formic acid at a flow rate of 400 nanoliters/minute (nL/min) at a column temperature of 55 °C. Data collection on the Fusion Lumos mass spectrometer was performed for three different compensation voltages (−40, −60, −80 v). Within each CV, a data-dependent acquisition (DDA) mode of acquisition with a $r = 120{,}000$ (@ m/z 200) full MS scan from m/z 375–1500 with a target AGC value of 4e5 ions was performed. MS/MS scans with HCD settings of 30% were acquired in the linear ion trap in "rapid" mode with a target AGC value of 1e4 and max fill time of 35 ms. The total cycle time for each CV was 0.66 s, with total cycle times of 2 s between like full MS scans. A 20 s dynamic exclusion was employed to increase depth of coverage. The total analysis cycle time for each sample injection was approximately 2 h.

Following 15 total UPLC-MS/MS analyses (excluding conditioning runs, but including 3 replicate SPQC samples), data were imported into Proteome Discoverer 3.0 (Thermo Scientific Inc.) and individual LCMS data files were aligned based on the accurate mass and retention time of detected precursor ions ("features") using Minora Feature Detector algorithm in Proteome Discoverer. Relative peptide abundance was measured based on peak intensities of selected ion chromatograms of the aligned features across all runs. The MS/MS data were searched against the SwissProt *Danio rerio* database, a common contaminant/spiked protein database (bovine albumin, bovine casein, yeast ADH, etc.), and an equal number of reversed-sequence "decoys" for false discovery rate determination. Sequest with INFERYS was utilized to produce fragment ion spectra and to perform the database searches. Database search parameters included fixed modification on Cys (carbamidomethyl) and variable modification on Met (oxidation). Search tolerances were 2 ppm precursor and 0.8 Da product ion with full trypsin enzyme rules. Peptide Validator and Protein FDR Validator nodes in Proteome Discoverer were used to annotate the data at a maximum 1% protein false discovery rate based on *q*-value calculations. Peptide homology was addressed using razor rules in which a peptide matched to multiple different proteins was exclusively assigned to the protein has more identified peptides. Protein homology was addressed by grouping proteins that had the same set of peptides to account for their identification. A master protein within a group was assigned based on % coverage. Prior to normalization, a filter was applied such that a peptide was removed if it was not measured at least twice across all samples and in at least 50% of the replicates in any one single group. After that filter, samples' total intensities were normalized (total intensity of all peptides for a sample are summed then normalized across all samples). Next, the following imputation strategy was applied to missing values. If less than half of the values were missing in a biological group, values were imputed with an intensity derived from a normal distribution of all values defined by measured values within the same intensity range (20 bins). If greater than half values were missing for a peptide in a group and a peptide intensity is >5e6, then it was concluded that the peptide was misaligned and its measured intensity is set to 0. All remaining missing values are imputed with the lowest 2% of all detected values. Peptide intensities were then subjected to a trimmed-mean normalization in which the top and bottom 10% of the signals were excluded and the average of the remaining values was used to normalize across all samples. Lastly, all peptides belonging to the same protein were then summed into a single intensity. These normalized protein intensities are what was used for the remainder of the analysis.

This dataset had a total of 54,694 unique peptides corresponding to 6336 unique proteins scored at a 1% FDR. Proteins with $p > 0.05$ and a change ≥1.5 fold were chosen for further analysis. Taken together, 1331 unique proteins displayed different levels between wild-type and *ddx61-KO* during heart regeneration. GO analyses were performed using DAVID Functional Annotation Bioinformatics Microarray Analysis and PANTHER knowledgebase. Cytoscape and STRING and BioGRID databases were used for interactome analyses.

eCLIP-seq profiling

For the eCLIP-seq assay, heart injuries were performed using the Z-CAT ablation model described earlier. Hearts were collected 14 days post tamoxifen treatment. 120 zebrafish hearts were extracted for each sample and immediately flash frozen on dry ice. Samples were then

processed as previously described[52]. Briefly, samples were UV cross-linked, and co-IP of Ddx61 was performed using the anti-DDX6 antibody (Abclonal). Samples were then evaluated and purified by isolating RNA associated with the Ddx61 size after western blotting. The subsequent RNA samples were then reverse transcribed, and DNA linkers were added. Quality control was conducted by measuring samples by Qubit and Tapestation, and samples were analyzed by BGI Genomics and sequenced.

Sequencing data was analyzed using the CLIP Tool Kit (CTK) pipeline[63]. A total of 467 unique genes were identified for uninjured and 14 dpi hearts, of which 92 genes showed at least one read in each of the duplicates and more than 2 reads per gene. GO analyses were performed using DAVID Functional Annotation Bioinformatics Microarray Analysis and PANTHER knowledgebase.

Histology and imaging

Immunofluorescence and AFOG staining of zebrafish hearts were performed on 4% paraformaldehyde-fixed 10 µm cryosections as described previously[17]. Primary and secondary antibodies used in this study are summarized in Supplementary Data 7.

Immunofluorescence of mouse tissue was conducted similar to staining of zebrafish hearts. Briefly, 4% paraformaldehyde-fixed hearts were sectioned in 10 µm slices on slides and washed 3 times each 5 min in wash buffer (PBS + 0.1% Tween20 (TBST) + 10 % NGS + 1% DMSO) and subsequently blocked for 30 min at 37 °C. Primary antibodies were incubated for 3 h at 37 °C. After incubation, slides were washed 3 times each 5 min in wash buffer and secondary antibodies were incubated at 37 °C for 1 h. Slides were washed four times in wash buffer and were mounted with Vectashield (Vector).

Stained zebrafish tissue sections were imaged on a ZEISS LSM 700. STED super resolution images were obtained by using Leica DMi8 with STED lasers and three high sensitivity Hybrid Detectors from the Duke Light Microscopy Core facility. Imaris software was used to generate Movies 1–4. Sections stained by AFOG were imaged using a Leica DFC450C compound microscope. For super resolution of hiPSC-derived cardiomyocytes, structured illumination microscopy (SIM) was performed using a Zeiss ELYRA 7 system with Lattice SIM2. Image reconstruction was performed using Zeiss ZEN Blue software with the structured illumination processing module. Channel alignment was performed using 100 nm multi-spectral fluorescent beads (TetraSpeck, Thermo Fisher Scientific) with the channel alignment function in ZEN Blue.

For immunostaining of hiPSC cultures, samples were seeded onto Aclar® Coverslips (Ted Pella 10501) prior to differentiation or shRNA experiments. Samples were fixed for 10 min in 4% PFA at room temperature (RT), then incubated in a blocking buffer (5% donkey serum in 0.1% Triton PBS). Primary antibodies were diluted in blocking buffer at 1:100 for Ddx6, LSM14 and 4E-T, and 1:200 for cTnnT. Samples were incubated for 1 h at room temperature prior to incubation with donkey anti-rabbit 647 secondary antibody (1:1000) and Hoechst 33342 (1:100). Samples were mounted with ProLong Glass Antifade Mountant (Thermo P36984) and imaged with an Andor Dragonfly Spinning Disk Confocal microscope. For RNAscope, the Multiplex v2 kit and Vivid dye 570 from ACD Biosciences were used. 4% PFA fixed slides were stained according to the manufacturer's protocol. After RNAscope, IF staining for Ddx61 was conducted.

Quantification of condensate cluster size and number

Image J Fiji was used to quantify condensate cluster features. One 100 × 100 µm area (0.01 mm^2) was measured for each image of sectioned tissue or iPSC cultures. Condensate cluster size and number were determined by the signal area (see Fig. S1H). In short, a threshold for the background signal was set and used for analysis of a group (Z-CAT, Nrg1-OE, etc). Thresholds were set using images of the treated group rather than its control, to avoid background signal amplifications in treated samples. Next, the area of ROIs were measured. Condensate cluster sizes varied between experiments due to thresholding based on staining intensity and background. This automated quantification of confocal images likely overcalculates the sizes of condensate clusters due to poorer resolution and grouping of multiple condensate clusters when compared to STED images (see Fig. 1E–G vs Fig. 1M). Ten hearts were measured for zebrafish, 4 hearts were measured for mice (male and female, C57BL/6), and 9 images were analyzed for iPSC cell maturation. Prior to analysis, Blind Analysis Tools (Image J) was used to allow for unbiased analysis.

Quantification of cardiomyocyte cycling, epicardial cell cycling, and immature muscle marker expression

Cardiomyocyte cycling was determined by calculating a ratio of $PCNA^+Mef2^+$ cells per total $Mef2^+$ cells as previously described[64]. $Mef2^+$ and $PCNA^+Mef2^+$ nuclei were counted in a 100 µm region measured from the edge of ventricular muscle. Blind Analysis Tools (Image J) was used to allow for unbiased analysis. Sm22 signal quantification in wild-type and *ddx61-KO* hearts was performed as previously described[65]. Briefly, the Sm22/MHC area ratio was determined by measuring the area of the MHC signal in a 185 µm section from the edge of ventricular muscle using Image J. The Sm22 signal was then measured in this section and expressed as a ratio of the total MHC area. Prior to analysis, Image J's Blind Analysis Tools were used to allow for unbiased analysis.

RIP assay and RT-qPCR

Isolation of Ddx61-associated mRNAs was performed as described previously [66]. Briefly, 30 zebrafish hearts were collected and immediately frozen on dry ice. After collection, an equal volume of polysome lysis buffer was added and cells were separated using a pestle. Samples were flash frozen and incubated on ice for 15 min. After thawing, a pestle was used to break cells open and samples were centrifuged. No crosslinking agent was used; instead, the native RIP protocol was used to isolate Ddx61-associated transcripts. Western blot analysis was used to determine the efficiency of Ddx61 pulldown. After mRNA isolation, reverse transcription was performed and samples were analyzed for the presence of *chordin* and *GAPDH* mRNAs in Input and IP samples using qPCR. Normalization of *chordin* levels (Input/IP normalized) was performed to *GAPDH* (Input/IP normalized) mRNA levels. For qRT-PCR of *chrd* and *bmpr2a* the following published sequences were used: *chrd* [67] and *bmpr2a* [68].

Western blot analysis and quantification

Western blot analysis was performed as previously described[17]. In short, hearts were lysed in RIPA and 25 µg of protein were loaded onto the SDS-PAGE. Blotting was conducted at 4 °C overnight. Quantification of Western blot signals was performed using the gel analysis tool in Image J. For Western blot analysis of hiPSC-derived cardiomyocytes, protein samples were harvested in RIPA buffer containing 1:1000 Phosphatase Inhibitor Cocktail 3 (Sigma P0044) and 1:100 protease inhibitor cocktail (Sigma P8340). Twenty micrograms of protein per lane was run on Bolt™ 4–12%, Bis-Tris gels (Thermo NW04120) prior to transfer to 0.2 µm PVDF membranes. Membranes were blocked in 5% BSA in TBS, followed by incubation in primary antibody diluted in blocking buffer (1:1000 Cyclophilin B or 1:1000 DDX6) overnight at 4 °C. Secondary antibody (1:5000) was incubated for 2 h at RT. Membranes were exposed with SuperSignal™ West Pico PLUS Chemiluminescent Substrate (Thermo 34580) for 5 min prior to imaging. The BandPeakQuantification plugin (Image J) was used to quantify protein expression. For presentation of full scan blots, see the Source data.

Statistics

Biological replicates were used for all data, and all statistical values are represented as mean ± SEM. Mann–Whitney U tests were used for quantifications of condensate clusters, IF signals, and EdU

incorporation in sorted GFP⁺ CMs. Unpaired two-tailed *t*-tests were used for quantification of CM cycling, WB analyses, and cortical wall thickness. Fisher's exact tests were used for semiquantitative scoring of 30 dpa heart regeneration.

hiPSC-CM differentiation and culture

hiPSCs were differentiated to CMs as previously described[69,70]. Specifically, cells were cultured on culture dishes or Aclar® Coverslips (Ted Pella 10501) coated with Matrigel® hESC-Qualified Matrix (Corning 354277). hiPSCs were dissociated with Accutase (Stem Cell Technologies) and plated at a density of $0.64 \times 106/cm^2$ for differentiation in mTeSR+ (Stem Cell Technologies) media containing 5 μM Y-27632 (Tocris 1254) for 24 h, followed by mTeSR+ without Y-27632 for 48 days prior to induction of differentiation. On the day of differentiation, cells were incubated in RPMI-1640 media containing B27 minus insulin supplement (RB-, Thermo A1895601), 60 ng/mL activin A (Peprotech 120-14E), 12 μM Chir 99021 (Tocris 4423), and 50 μg/mL L-ascorbic acid 2-phosphate (Sigma A8960) for 24 h. Subsequently, RB- media containing 50 μg/mL ascorbic acid and 5 μM IWR-1 (Tocris 3532/10) was applied for 2 days, followed by removal of ascorbic acid on day 4. On day 6, cells were treated with RPMI-1640 with B27 containing insulin supplement (RB + , Thermo 17504044) for 48 h. On day 8, cells were subjected for 48 h to metabolic selection media containing glucose-free RPMI (Thermo 11879020), 4 mM lactate (Sigma L4263), 0.5 mg/mL recombinant human albumin (Sigma A6612), and 213 μg/mL L-ascorbic acid 2-phosphate (Sigma A8960)[71]. CMs were maintained thereafter in 3DRB+ medium (RB+ containing 2 mg/mL aminocaproic acid (Sigma A2504), 50 mg/mL ascorbic acid (Sigma A8960), 0.45 μM thioglycerol (Sigma M6145), 1% Pen/Strep (Thermo 15070063), 1% non-essential amino acids (Thermo 11140050), and 1% sodium pyruvate (Thermo 11360070)) until used, as previously described[70].

Lentivirus production

Lentiviral plasmids containing U6 shRNA and hPGK eGFP inserts were ordered from VectorBuilder (Scramble Vector ID VB010000-0001mty, Ddx6 Vector ID VB230518-1255kbu). The knockdown efficacy of target sequence CGCAATCTTGTTTGCACTGAT for human Ddx6 was described previously[27]. Lentiviruses were generated as previously described[72]. Briefly, Hek293T cells (ATCC) were cultured to 60–80% confluence prior to transfection with vector plasmid (Scramble shRNA, Ddx6 shRNA, or MHCK7 H2B-mCherry reporter), packaging plasmid psPAX2 and envelope plasmid pMD2.G (2:1:1 mass ratios) using JetPrime Transfection reagent (PolyPlus). Culture medium was changed 12–16 h post-transfection, followed by harvest of media containing viral particles 48–72 h post-transfection. Viral particles were concentrated via centrifugation at 1500 x *g* for 45 min following overnight incubation with 1 part PEG solution (40% PEG 8000, 24 g/L NaCl) to 3 parts virus-containing medium. Lentivirus was stored at −80 °C prior to use.

Flow cytometry

MHCK7 H2B-mCherry and shRNA eGFP lentiviruses were applied at a MOI of 0.8–1. 5-ethynyl-2′-deoxyuridine (EdU) was delivered at 10 μM concentration for the final 48 h prior to fixation for flow cytometry. Cells were trypsinized for 3.5 min prior to fixation with 2% PFA at RT for 10 min. Cells were subsequently stained with Click-iT™ EdU Alexa Fluor™ 647 Flow Cytometry Assay Kit (Thermo C10419) and incubated with Hoechst 33342 prior to analysis. Cells were analyzed on a FortessaX20 flow cytometer. Using FlowJo software, cells were gated for GFP (shRNA+) and H2B mCherry (CMs), and Hoechst (DNA content). EdU was analyzed in the shRNA+ CM population.

DDX6 overexpression

For *DDX6* overexpression, Addgene plasmid 119947 (phage UbiC tagRFP-T-DDX6 was a gift from Jeffrey Chao, Addgene plasmid # 119947; http://n2t.net/addgene:119947; RRID:Addgene_119947) was used to generate lentivirus. To generate the RFP control vector, the Ddx6 coding sequence was excised from the same plasmid. Cells were transduced with RFP or Ddx6-RFP viruses at an MOI of 0.7–0.9, 4 days prior to experimental endpoints for imaging, flow cytometry, and Western blot. For EdU incorporation assays, D2 mesoderm cells were incubated with 10 mM EdU for 2 h, while D28 CMs were incubated with 10 mM EdU for 48 h.

FRAP assay and analysis

FRAP experiments were performed using an Andor Dragonfly spinning disk confocal microscope equipped with a 63×/1.4 NA oil immersion objective and environmental control (37 °C, 5% CO_2). Cells were seeded in 35 mm glass-bottom dishes (ibidi) and transduced with RFP or Ddx6-RFP lentivirus 4 days prior to imaging. Prior to imaging, medium was replaced with pre-warmed RPMI supplemented with 20 mM HEPES + 10 μM blebbistatin. FRAP experiments were conducted using Andor Mosaic software. Pre-bleach images were acquired for 5 frames at 10-s intervals. Photobleaching was performed using 100% laser power for 15 s. Post-bleach images were acquired at 10-s intervals. FRAP analysis was conducted as described[73].

Reporting summary

Further information on research design is available in the Nature Portfolio Reporting Summary linked to this article.

Data availability

The eCLIP-seq dataset generated in this study have been deposited in the Gene Expression Omnibus (GEO) archive GSE246577. BioID2 and *ddx61* datasets are available via ProteomeXchange with identifier PXD046501. Source data are provided with this paper.

References

1. Goldman, J. A. et al. Resolving heart regeneration by replacement histone profiling. *Dev. Cell* **40**, 392–404 e395 (2017).
2. Kang, J. et al. Modulation of tissue repair by regeneration enhancer elements. *Nature* **532**, 201–206 (2016).
3. Guenther, C. A. et al. A distinct regulatory region of the Bmp5 locus activates gene expression following adult bone fracture or soft tissue injury. *Bone* **77**, 31–41 (2015).
4. Wang, W. et al. Changes in regeneration-responsive enhancers shape regenerative capacities in vertebrates. *Science* **369**,eaaz3090 (2020).
5. Harris, R.E., Setiawan, L., Saul, J. & Hariharan, I.K. Localized epigenetic silencing of a damage-activated WNT enhancer limits regeneration in mature Drosophila imaginal discs. *Elife* **5**, e11588 (2016).
6. Vizcaya-Molina, E. et al. Damage-responsive elements in Drosophila regeneration. *Genome Res.* **28**, 1852–1866 (2018).
7. Rao, A. et al. The translation initiation factor homolog eif4e1c regulates cardiomyocyte metabolism and proliferation during heart regeneration. *Development* **150**, dev201376 (2023).
8. Yin, V. P. et al. Fgf-dependent depletion of microRNA-133 promotes appendage regeneration in zebrafish. *Genes Dev.* **22**, 728–733 (2008).
9. Tian, Y. et al. A microRNA-Hippo pathway that promotes cardiomyocyte proliferation and cardiac regeneration in mice. *Sci. Transl. Med.* **7**, 279ra238 (2015).
10. Walker, S.E., Sabin, K.Z., Gearhart, M.D., Yamamoto, K. & Echeverri, K. Regulation of stem cell identity by miR-200a during spinal cord regeneration. *Development* **149**, dev200033 (2022).
11. Subramanian, E. et al. A small noncoding RNA links ribosome recovery and translation control to dedifferentiation during salamander limb regeneration. *Dev. Cell* **58**, 450–460 e456 (2023).
12. Porrello, E. R. et al. Regulation of neonatal and adult mammalian heart regeneration by the miR-15 family. *Proc. Natl. Acad. Sci. USA* **110**, 187–192 (2013).

13. Poss, K. D., Wilson, L. G. & Keating, M. T. Heart regeneration in zebrafish. *Science* **298**, 2188–2190 (2002).
14. Garcia-Puig, A. et al. Proteomics analysis of extracellular matrix remodeling during zebrafish heart regeneration. *Mol. Cell Proteom.* **18**, 1745–1755 (2019).
15. Wang, J., Karra, R., Dickson, A. L. & Poss, K. D. Fibronectin is deposited by injury-activated epicardial cells and is necessary for zebrafish heart regeneration. *Dev. Biol.* **382**, 427–435 (2013).
16. Ma, D. et al. Dynamics of zebrafish heart regeneration using an HPLC-ESI-MS/MS approach. *J. Proteome Res.* **17**, 1300–1308 (2018).
17. Pronobis, M.I., Zheng, S., Singh, S.P., Goldman, J.A. & Poss, K.D. In vivo proximity labeling identifies cardiomyocyte protein networks during zebrafish heart regeneration. *Elife* **10**, e66079 (2021).
18. Gemberling, M., Karra, R., Dickson, A.L. & Poss, K.D. Nrg1 is an injury-induced cardiomyocyte mitogen for the endogenous heart regeneration program in zebrafish. *Elife* **4**, e05871 (2015).
19. Karra, R. et al. Vegfaa instructs cardiac muscle hyperplasia in adult zebrafish. *Proc. Natl. Acad. Sci. USA* **115**, 8805–8810 (2018).
20. Han, Y. et al. Vitamin D stimulates cardiomyocyte proliferation and controls organ size and regeneration in zebrafish. *Dev. Cell* **48**, 853–863 e855 (2019).
21. Bertozzi, A., Wu, C. C., Hans, S., Brand, M. & Weidinger, G. Wnt/beta-catenin signaling acts cell-autonomously to promote cardiomyocyte regeneration in the zebrafish heart. *Dev. Biol.* **481**, 226–237 (2022).
22. Zhao, L., Ben-Yair, R., Burns, C. E. & Burns, C. G. Endocardial notch signaling promotes cardiomyocyte proliferation in the regenerating zebrafish heart through Wnt pathway antagonism. *Cell Rep.* **26**, 546–554.e5 (2019).
23. D'Uva, G. et al. ERBB2 triggers mammalian heart regeneration by promoting cardiomyocyte dedifferentiation and proliferation. *Nat. Cell Biol.* **17**, 627–638 (2015).
24. Brengues, M., Teixeira, D. & Parker, R. Movement of eukaryotic mRNAs between polysomes and cytoplasmic processing bodies. *Science* **310**, 486–489 (2005).
25. Coller, J. M., Tucker, M., Sheth, U., Valencia-Sanchez, M. A. & Parker, R. The DEAD box helicase, Dhh1p, functions in mRNA decapping and interacts with both the decapping and deadenylase complexes. *RNA* **7**, 1717–1727 (2001).
26. Parker, R. & Sheth, U. P bodies and the control of mRNA translation and degradation. *Mol. Cell* **25**, 635–646 (2007).
27. Di Stefano, B. et al. The RNA helicase DDX6 controls cellular plasticity by modulating P-body homeostasis. *Cell Stem Cell* **25**, 622–638 e613 (2019).
28. Shimada, R., Kiso, M. & Saga, Y. ES-mediated chimera analysis revealed requirement of DDX6 for NANOS2 localization and function in mouse germ cells. *Sci. Rep.* **9**, 515 (2019).
29. Hondele, M. et al. DEAD-box ATPases are global regulators of phase-separated organelles. *Nature* **573**, 144–148 (2019).
30. Carroll, J. S., Munchel, S. E. & Weis, K. The DExD/H box ATPase Dhh1 functions in translational repression, mRNA decay, and processing body dynamics. *J. Cell Biol.* **194**, 527–537 (2011).
31. Wang, J. et al. The regenerative capacity of zebrafish reverses cardiac failure caused by genetic cardiomyocyte depletion. *Development* **138**, 3421–3430 (2011).
32. Sheth, U. & Parker, R. Decapping and decay of messenger RNA occur in cytoplasmic processing bodies. *Science* **300**, 805–808 (2003).
33. Cougot, N., Babajko, S. & Seraphin, B. Cytoplasmic foci are sites of mRNA decay in human cells. *J. Cell Biol.* **165**, 31–40 (2004).
34. Kshirsagar, M. & Parker, R. Identification of Edc3p as an enhancer of mRNA decapping in *Saccharomyces cerevisiae*. *Genetics* **166**, 729–739 (2004).
35. Blobel, G. & Sabatini, D. Dissociation of mammalian polyribosomes into subunits by puromycin. *Proc. Natl. Acad. Sci. USA* **68**, 390–394 (1971).
36. Eulalio, A., Behm-Ansmant, I., Schweizer, D. & Izaurralde, E. P-body formation is a consequence, not the cause, of RNA-mediated gene silencing. *Mol. Cell Biol.* **27**, 3970–3981 (2007).
37. Brandmann, T. et al. Molecular architecture of LSM14 interactions involved in the assembly of mRNA silencing complexes. *EMBO J.* **37**, e97869 (2018).
38. Kamenska, A. et al. The DDX6-4E-T interaction mediates translational repression and P-body assembly. *Nucleic Acids Res.* **44**, 6318–6334 (2016).
39. Minshall, N., Reiter, M. H., Weil, D. & Standart, N. CPEB interacts with an ovary-specific eIF4E and 4E-T in early Xenopus oocytes. *J. Biol. Chem.* **282**, 37389–37401 (2007).
40. Yang, W. H., Yu, J. H., Gulick, T., Bloch, K. D. & Bloch, D. B. RNA-associated protein 55 (RAP55) localizes to mRNA processing bodies and stress granules. *RNA* **12**, 547–554 (2006).
41. Hubstenberger, A. et al. P-body purification reveals the condensation of repressed mRNA regulons. *Mol. Cell* **68**, 144–157 e145 (2017).
42. Tanner, N. K., Cordin, O., Banroques, J., Doere, M. & Linder, P. The Q motif: a newly identified motif in DEAD box helicases may regulate ATP binding and hydrolysis. *Mol. Cell* **11**, 127–138 (2003).
43. Jumper, J. et al. Highly accurate protein structure prediction with AlphaFold. *Nature* **596**, 583–589 (2021).
44. Mugler, C.F. et al. ATPase activity of the DEAD-box protein Dhh1 controls processing body formation. *Elife* **5**, e18746 (2016).
45. Kim, J. et al. The RNA helicase DDX6 controls early mouse embryogenesis by repressing aberrant inhibition of BMP signaling through miRNA-mediated gene silencing. *PLoS Genet.* **18**, e1009967 (2022).
46. Kubin, T. et al. Oncostatin M is a major mediator of cardiomyocyte dedifferentiation and remodeling. *Cell Stem Cell* **9**, 420–432 (2011).
47. Bassat, E. et al. The extracellular matrix protein agrin promotes heart regeneration in mice. *Nature* **547**, 179–184 (2017).
48. Soonpaa, M. H., Kim, K. K., Pajak, L., Franklin, M. & Field, L. J. Cardiomyocyte DNA synthesis and binucleation during murine development. *Am. J. Physiol.* **271**, H2183–H2189 (1996).
49. de Carvalho, A. et al. Early postnatal cardiomyocyte proliferation requires high oxidative energy metabolism. *Sci. Rep.* **7**, 15434 (2017).
50. Li, X. et al. Inhibition of fatty acid oxidation enables heart regeneration in adult mice. *Nature* **622**, 619–626 (2023).
51. Wang, Z. et al. Cell-type-specific gene regulatory networks underlying murine neonatal heart regeneration at single-cell resolution. *Cell Rep.* **33**, 108472 (2020).
52. Van Nostrand, E. L. et al. Robust transcriptome-wide discovery of RNA-binding protein binding sites with enhanced CLIP (eCLIP). *Nat. Methods* **13**, 508–514 (2016).
53. Wang, C. et al. Context-dependent deposition and regulation of mRNAs in P-bodies. *Elife* **7**, e29815 (2018).
54. Aizer, A. et al. Quantifying mRNA targeting to P-bodies in living human cells reveals their dual role in mRNA decay and storage. *J. Cell Sci.* **127**, 4443–4456 (2014).
55. Courel, M. et al. GC content shapes mRNA storage and decay in human cells. *Elife* **8**, e49708 (2019).
56. Wu, C. C. et al. Spatially resolved genome-wide transcriptional profiling identifies BMP signaling as essential regulator of zebrafish cardiomyocyte regeneration. *Dev. Cell* **36**, 36–49 (2016).
57. Tucker, J. A., Mintzer, K. A. & Mullins, M. C. The BMP signaling gradient patterns dorsoventral tissues in a temporally progressive manner along the anteroposterior axis. *Dev. Cell* **14**, 108–119 (2008).
58. Gallo, C. M., Munro, E., Rasoloson, D., Merritt, C. & Seydoux, G. Processing bodies and germ granules are distinct RNA granules that interact in C. elegans embryos. *Dev. Biol.* **323**, 76–87 (2008).
59. Suh, N. et al. MicroRNA function is globally suppressed in mouse oocytes and early embryos. *Curr. Biol.* **20**, 271–277 (2010).

60. Su, Y. Q. et al. Selective degradation of transcripts during meiotic maturation of mouse oocytes. *Dev. Biol.* **302**, 104–117 (2007).
61. Chekulaeva, M., Hentze, M. W. & Ephrussi, A. Bruno acts as a dual repressor of oskar translation, promoting mRNA oligomerization and formation of silencing particles. *Cell* **124**, 521–533 (2006).
62. Chicoine, J. et al. Bicaudal-C recruits CCR4-NOT deadenylase to target mRNAs and regulates oogenesis, cytoskeletal organization, and its own expression. *Dev. Cell* **13**, 691–704 (2007).
63. Shah, A., Qian, Y., Weyn-Vanhentenryck, S. M. & Zhang, C. CLIP tool Kit (CTK): a flexible and robust pipeline to analyze CLIP sequencing data. *Bioinformatics* **33**, 566–567 (2017).
64. Wang, J. & Poss, K. D. Methodologies for inducing cardiac injury and assaying regeneration in adult zebrafish. *Methods Mol. Biol.* **1451**, 225–235 (2016).
65. Ogawa, M. et al. Kruppel-like factor 1 is a core cardiomyogenic trigger in zebrafish. *Science* **372**, 201–205 (2021).
66. Gagliardi, M. & Matarazzo, M. R. RIP: RNA immunoprecipitation. *Methods Mol. Biol.* **1480**, 73–86 (2016).
67. Branam, A. M., Hoffman, G. G., Pelegri, F. & Greenspan, D. S. Zebrafish chordin-like and chordin are functionally redundant in regulating patterning of the dorsoventral axis. *Dev. Biol.* **341**, 444–458 (2010).
68. Wu, Y., Sun, A., Nie, C., Gao, Z. X. & Wan, S. M. Functional differentiation of bmp2a and bmp2b genes in zebrafish. *Gene Expr. Patterns* **46**, 119288 (2022).
69. Jackman, C. P., Carlson, A. L. & Bursac, N. Dynamic culture yields engineered myocardium with near-adult functional output. *Biomaterials* **111**, 66–79 (2016).
70. Shadrin, I. Y. et al. Cardiopatch platform enables maturation and scale-up of human pluripotent stem cell-derived engineered heart tissues. *Nat. Commun.* **8**, 1825 (2017).
71. Burridge, P. W. et al. Chemically defined generation of human cardiomyocytes. *Nat. Methods* **11**, 855–860 (2014).
72. Nguyen, H. X., Kirkton, R. D. & Bursac, N. Engineering prokaryotic channels for control of mammalian tissue excitability. *Nat. Commun.* **7**, 13132 (2016).
73. Pronobis, M. I., Rusan, N. M. & Peifer, M. A novel GSK3-regulated APC:Axin interaction regulates Wnt signaling by driving a catalytic cycle of efficient betacatenin destruction. *Elife* **4**, e08022 (2015).

Acknowledgements

We thank the Duke Zebrafish Core for animal care; F. Conlon, C. Nicchitta, J. Cao, and M. Bagnat for helpful comments on the manuscript; B. Capel for tissue samples; and M. Mullins for sharing transgenic animals. We thank the Duke Proteomics and Metabolomics Core for assistance with the BioID2 assay and proteomics, the Duke Light Microscopy Core Facility, and the Duke Cancer Institute Flow Cytometry Shared Resource. This work was supported by Life Science Research Foundation—Astellas Pharma (M.I.P.). American Heart Association Career Development Award 937678 (M.I.P.), Start-up funding University of Denver (M.I.P.), National Institutes of Health predoctoral fellowship 1F31HL162460 (S.D.), National Institutes of Health grant U01HL134764 (N.B.), National Institutes of Health grant R01HL164013 (N.B.), National Institutes of Health grant R35 HL150713 (K.P.), American Heart Association Merit Award (K.P.), National Institutes of Health S10: 1S10OD28703-01 (Duke LMCF).

Author contributions

Conceptualization: M.I.P. and K.D.P.; Methodology: M.I.P., S.D., and S.L.; Investigation: M.I.P., S.D., S.L., and L.G.; Visualization: M.I.P. and J.O.; Funding acquisition: M.I.P., K.D.P., and N.B.; Project administration: K.D.P. and N.B.; Supervision: K.D.P. and N.B.; Writing—original draft: M.I.P. and K.D.P.; Writing—review and editing: M.I.P. and K.D.P.

Competing interests

The authors declare no competing interests.

Additional information

Supplementary information The online version contains supplementary material available at https://doi.org/10.1038/s41467-025-64026-5.

Correspondence and requests for materials should be addressed to Kenneth D. Poss.

Peer review information *Nature Communications* thanks Peiheng Gan and the other anonymous reviewer(s) for their contribution to the peer review of this work. A peer review file is available.

Reprints and permissions information is available at http://www.nature.com/reprints

Publisher's note Springer Nature remains neutral with regard to jurisdictional claims in published maps and institutional affiliations.

Open Access This article is licensed under a Creative Commons Attribution-NonCommercial-NoDerivatives 4.0 International License, which permits any non-commercial use, sharing, distribution and reproduction in any medium or format, as long as you give appropriate credit to the original author(s) and the source, provide a link to the Creative Commons licence, and indicate if you modified the licensed material. You do not have permission under this licence to share adapted material derived from this article or parts of it. The images or other third party material in this article are included in the article's Creative Commons licence, unless indicated otherwise in a credit line to the material. If material is not included in the article's Creative Commons licence and your intended use is not permitted by statutory regulation or exceeds the permitted use, you will need to obtain permission directly from the copyright holder. To view a copy of this licence, visit http://creativecommons.org/licenses/by-nc-nd/4.0/.

© The Author(s) 2025